3D Hydrogel Formation via a Radical-free and Multiphoton-mediated Oxime Ligation

Nicholas Ka-Kit Lai

A thesis

submitted in partial fulfillment of the

requirements for the degree of

Master of Science

University of Washington

2025

Committee:

Cole A. DeForest

Zachary Sherman

Program Authorized to Offer Degree:

Department of Chemical Engineering

University of Washington

Abstract

3D Hydrogel Formation via a Radical-free and Multiphoton-mediated Oxime Ligation

Nicholas Ka-Kit Lai

Chair of the Supervisory Committee:

Cole A. DeForest

Department of Chemical Engineering

Light is a unique stimulus with high bioorthogonality, enabling spatiotemporal control in the creation and modification of biomaterials. Photopolymerization permits solid materials to be formed from liquid precursors upon directed light exposure. This technique is valuable in the field of tissue engineering due to its ability to create complex structures with high levels of control. Additionally, light's compatibility with living systems enables cells to be encapsulated within photopolymerized 3D materials, creating a more replicative environment than traditional 2D cultures, and provides a route towards 4D customization with structures that can vary in both time and 3D space. While this technique improves the programmability of hydrogel formation, many photopolymerizations produce free radicals that can be cytotoxic and cause undesired reactions due to their highly reactive nature. Herein, we introduce and utilize a method to create 3D hydrogels via a radical-free and multiphoton-mediated oxime ligation.

Main Text:

Hydrogels are water-swollen polymeric networks that are broadly used due to their biocompatibility and tunable characteristics. They can be engineered to mimic physical and chemical aspects of native tissue due to their mechanical similarity with tissue and high water content[1]. To further mimic the dynamic heterogeneity of cellular microenvironments, current-generation cell culture platforms have high demand for biomaterials that can offer spatiotemporal control beyond the fixed 3D matrices[2]. To address the need for a bioorthogonal, high-control stimuli, light serves as a powerful tool that enables precise control over when, where, and the extent of modification in a dose-dependent manner. Utilizing the uniqueness of light, photochemistry provides additional tunability and customizations to hydrogel fabrication over both time and space (i.e., 4D).

Light-based fabrication enables direct user-customization of hydrogels with high resolution and geometric complexity. Recent developments include single photon-based fabrication, volumetric printing, and multiphoton lithography. Single-photon stereolithography (SLA) uses raster-scanning laser to polymerize 2D shapes at each layer. Like SLA, Digital Light Processing (DLP) also relies on single-photon responsive materials for hydrogel customization, but in a different patterning style. DLP utilizes multiple micromirrors to control the incoming light to generate a projected image and illuminates the entire 2D region of interest layer-by-layer. Although both techniques offer high-resolution print (~10 μm)[3,4], their layer-based patterning nature can cause potential long print time and hinder the ability to build complex geometries. Unlike SLA/DLP, volumetric printing enables photoreactions in 3D *via* tomography at a much faster speed. Prepolymer solutions are illuminated at different angles through rotating the samples or with multiple light sources, motivating photopolymerization at desire location[5–7]. This approach can

fabricate centimeter-scale acrylic with feature size of ~80 μm in ~20 s[5]. Although SLA/DLP and volumetric printing can produce tissue-scale structures, neither can reach the subcellular resolution necessary to fully mimic the extracellular matrix (ECM). In addition, these techniques have limited ability to perform gradient fabrication, hindering the ability to replicate the heterogeneity of native tissue.

Multiphoton lithography is a technique which utilizes the near-simultaneous absorption of two or more photons at the laser's focal point to enable high precision 3D micro-scale patterning within photoresponsive materials. The modification is confined to the focal point and non-focused regions remain unaffected, offering precise spatial controls to generate intricate 3D geometries in hydrogel. Despite the longer fabrication times than techniques previously mentioned, the ability to achieve subcellular resolution provides a more precise model of the ECM. Early application of this technique was used for photomediated hydrogel formation and cell guidance/migration with peptide-modified hydrogels[8]. In addition, multiphoton lithography can also be used for hydrogel photoablation to create more complex structures[9,10]. Building upon multiphoton lithography and utilizing the light dose-dependent photochemistry, our group developed "grayscale image z-stack-guided multiphoton optical-lithography" (GIZMO) to better mimic the heterogeneity of the ECM[11]. GIZMO achieves complex subcellular resolution by varying laser intensity during raster scanning based on the inputted grayscale image stacks.

A key factor for photopolymerization is the presence of either photoinitiators or photolabile functional groups. Photoinitiator generates reactive species in response to light, either cleaves into two radicals (Type I) or generates radicals with co-initiators in the system (Type II)[12]. Type I photoinitiation processes rapidly and is highly efficient, but it requires high energy UV light for bond cleavage[13]. Lithium phenyl-2,4,6-trimethylbenzoylphosphinate (LAP) is a well-known type

I photoinitiator due to its high water solubility and cytocompatible violet light-sensitivity[12]. In contrast, type II photoinitiation is responsive to lower energy visible light, but it proceeds more slowly and is less efficient due to bimolecular reactions between the excited state photoinitiators and co-initiators. Methylene blue is used in Type II photopolymerization with triethanolamine as a co-initiator to fabricate colorless hydrogels[14]. In addition, some photoinitiators are capable of absorbing two photons at lower energy light, enabling two-photon polymerization. P2CK, a water soluble, cyclic benzylidene ketone-based type II photoinitiator has demonstrated the ability to facilitate photopolymerization[15]. However, the presence of radicals is not ideal for biological applications such as cell culturing. As a result, there is growing interest in developing new photopolymerizable chemistries that proceed cytocompatibly and in a radical-free manner.

Among photolabile groups, photocages are commonly used for inactivating the bonded species and dissociate upon light exposure, enabling the reactive groups to interact. *Ortho*-nitrobenzyl (*o*NB) is a popular choice among photocages due to its versatility with multiple functional groups[16]. 2-(2-Nitrophenyl) propyloxycarbonyl (NPPOC), an *o*NB photocage that protects amine groups and cleaves upon UV light was used for controlling oxime ligation[17]. Alternatively, coumarins serve as a great photocages due to their two-photon sensitivity, high wavelength absorption, and biocompatibility[18]. 7-dicarboxymethylaminocoumarin (DCMAC)'s high two-photon sensitivity enables control over hydrogel biochemical modification (but critically not yet for hydrogel formation) at high 3D resolution via multiphoton lithography[19,20]. In addition, DCMAC is cleaved upon two-photon stimulation at near-infrared range (~770 nm), increasing biocompatibility in contrast to the UV sensitive photocages. DCMAC is also highly water soluble, which reduces unwanted aggregation and/or phase separation to maintain a uniform crosslinking structure.

Step-growth polymerization is often preferred for hydrogel formation over the chain-growth approach due to its uniform microstructures and typically proceed without radicals, resulting in a more mechanically stable replicate of the ECM. Although many step-growth chemistries were considered uncontrollable due to their click reaction-like nature, photochemistry enables programmability on hydrogel fabrication. Thiol-ene reaction involves radical-mediated reaction between a thiol and an alkene. The Anseth group demonstrated that multiarm polymers end-functionalized with norbornene (NB), a highly strained bicyclic alkene, can form hydrogels via step-growth, radical-mediated photopolymerization with dithiol-crosslinkers. The reaction minimizes cytotoxicity as it requires less active radical concentration than chain-growth chemistry[21]. To go beyond the radical-mediated photochemistry, works were built on top of well-established spontaneous step-growth chemistries that were considered uncontrollable.

The Bertozzi group developed strain-promoted azide-alkyne cycloaddition (SPAAC), which utilizes the ring strain within the alkyne to drives the reaction forward under physiological conditions in the presence of azide[22]. This mechanism is highly biocompatible due to its limited reaction with natural biomolecules, opening the door to bioorthogonality. Multiphoton-activable SPAAC was later introduced by inactivating the strained-alkyne group with a photocaging cyclopropenone group[23]. The cyclopropenone will photouncage upon exposure to near-infrared light, subsequently permitting the spontaneous SPAAC reaction.

Oxime ligation has proven to be an attractive click reaction for hydrogel formation and does not rely on the propagation of free radicals, providing high biocompatibility and reaction specificity[17,24,25]. In oxime ligation, alkoxyamine reacts with an aldehyde or ketone to form an oxime linkage and a water byproduct. The reaction kinetics can be controlled by tuning the pH and aniline concentration[26]. Although the spontaneous nature of click reactions restricts them with

respect to spatiotemporal control, alkoxyamine photocaging has been demonstrated as an effective solution that endows this uniquely powerful click reaction with photoresponsiveness[17,27,28].

Towards establishing a radical-free and multiphoton-polymerizable hydrogel formulation, we sought to functionalize multi-arm poly(ethylene glycol) (PEG) cross-linkers with either DCMAC-photocaged alkoxyamine (-ON-DCMAC) or benzaldehyde (-CHO) and subsequently form hydrogels via photomediated oxime ligation. Moreover, DCMAC's uncaging has been shown to proceed rapidly and in a highly predictable dose-dependent manner, opening the door for large-scale grayscale hydrogel formation/stiffening via "grayscale image z-stack-guided multiphoton optical-lithography" (GIZMO)[11]. An orthogonal primary SPAAC network formed by PEG-bicyclononyne (PEG-BCN) and tetra(ethylene glycol)-diazide (TEG-diN_3) or thiol-ene network formed by PEG-NB and dithiothreitol (DTT) is introduced to increase the mechanical stability of hydrogel during patterning and improve the resolution of the patterns by preventing the precursors from moving freely. Despite the thiol-ene chemistry introducing free radical initiators, it had been shown that redox reaction via a low concentration of ammonium persulfate (APS)/tetramethylethylenediamine (TEMED) can still be cytocompatible[29]. PEG-ON-DCMAC and PEG-CHO are premixed with the primary network precursors, forming a gel (via SPAAC or thiol-ene) before the photopolymerizing process (**Figure 1a**). Furthermore, by replacing the TEG-diN_3 and DTT with diazide- and dicysteine-containing peptides respectively, the primary network can be enzymatically degraded to recover the oxime-patterned secondary network[30] (**Figure 1b**). In addition, photochemistry of DCMAC is characterized to evaluate the cleavage efficiency under various wavelengths and light intensity conditions.

Experimental Result:

Single-Photon Photokinetic characterization

Photomediated oxime linkage depends on the efficiency of photocage cleavage, which is influenced by both wavelength and light intensity. Photokinetic properties of DCMAC-photocaged alkoxyamine can characterize the cleavage efficiency of the photocage. To evaluate this, we exposed DCMAC-NO-N_3 to a range of light doses across different wavelengths and quantified the relative extent of uncaging via liquid chromatography-mass spectrometry (LC-MS) (Method. 1). The uncaged DCMAC alcohol byproducts were integrated for kinetic quantification (Method. 2). The results indicate that light dosage required for effective uncaging increases with longer wavelengths (**Figure 1c**). We also vary light intensity at 400 nm to observe the effect on photocleavage efficiency. As predicted, the dosage required for photocleavage remains unchanged at different power intensities (**Figure 1d**). After converting dosage into a time-dependent variable by the corresponding intensity used, the result suggests cleavage time scales linearly with light intensity, faster uncaging at higher light intensity.

In addition, single-photon quantum yield of DCMAC photouncaging can be estimated with photokinetic data[31,32]. The quantum yield of photouncaging describes the photon conversion efficiency (number molecules uncaged per number of photons absorbed). Since the result of our photoreaction suggest a first-order kinetic, quantum yield can be estimated using the rate constant and extinction coefficient of DCMAC at a known wavelength and power intensity (**Figure 1e**). We hypothesized that the single-photon quantum yield can help determine the two-photon absorption cross section (the probability of simultaneous absorption of two photons by the molecule) of the photocage.

Interpenetrating network 2-photon patterning

The SPAAC or thiol-ene primary network is initially formed while containing the precursors of the oxime secondary network (**Figure 1a**, Method. 3). Upon two-photon excitation, DCMAC is cleaved and the alkoxyamine undergoes oxime ligation with the benzaldehyde moieties. We first generated calibration grids to determine the amount of light required to form the secondary network (1, 3, 5, and 10 repeats with linear scanner) (**Figure 2a**). Next, we performed grayscale photopolymerization to demonstrate the ability to control local stiffness of the hydrogel. Toward

this goal, oxime-crosslinked networks were created in the form of "View of the Brenta, near Dolo" (**Figure 2b**). In addition, we also created a "flipbook" following inputted frames from a space shuttle launching video, consisting of 400 planar images (450μm x 450 μm x 400 μm) (**Figure 2c**). These patterned structures exhibit submicron resolution, demonstrating the precision of our photopatterning technique and the ability to customize hydrogel network with spatial control of intricate subcellular scale structures with grayscale, which we hypothesize to have different stiffnesses.

Patterned structures release through degradable primary network

We also showed the ability to degrade the primary network by implementing existing mechanisms[30]. The interpenetrating network can reduce into a single network through sortase-mediated degradation through implementing eSrtA(4S9) sortase-sensitive sequence on the crosslinkers in the primary network. The 4S9-sensitive sequence "LPESG" is embedded to the diazide and dicysteine crosslinkers. Following degradation of the primary network and diffusion of inactivated photocaged precursors, the light-exposed regions of the oxime-crosslinked network remain bonded. This allows us to release the patterned structures on the oxime-crosslinked network (**Figure 3ab**). To further illustrate the complexity of patterning that can be achieved, we also constructed a 3D egg structure within the gel (**Figure 3c**). Primary network degradation highlights the tunability of the interpenetrating network system, allowing clear visualization and direct interaction with the patterned structures for additional manipulation, such as cell encapsulation.

Discussion/Conclusion:

In this work, we demonstrated the ability to generate subcellularly structured materials with DCMAC-photocage-based oxime ligation via two-photon polymerization. Single-photon photokinetic studies demonstrate the reaction's varying visible light dose-dependence, a feature we exploit to achieve regional stiffness control of hydrogel fabrication. Although our photokinetic analysis has only been performed following single-photon excitation, we anticipate similar principle applies to two-photon polymerization as demonstrated by varying laser intensity via GIZMO to gain 4D control on hydrogel fabrication.

In our photomediated oxime ligation, fluorescent dye was only used on the primary network to determine patterned region due to photobleaching of the dye. Dye is not required to visualize the patterned structures on the oxime ligation network. Instead, the patterns were visible when imaging the secondary network at 405 nm, a wavelength which causes DCMAC to fluoresce. This observation is particularly interesting because we would typically expect both the photouncaged DCMAC and any unreacted DCMAC-photocaged alkoxyamine to diffuse out of the hydrogel after PBS washing. We hypothesize this may result from the accumulation of residual uncaged species due to the dose-dependent nature of photocleavage, or potential dimerization of photocages. However, dimerization should not significantly affect hydrogel formation since oxime ligation primarily depends on the presence of aniline.

The use of DCMAC for photomediated oxime ligation interpenetrating a degradable crosslinking network offers a promising approach to 3D hydrogel formation, circumventing the cytotoxicity associated with free radicals while providing rapid spatiotemporal control. Moving forward, we anticipate the oxime ligation networks are biocompatible for cell encapsulation, replicating the structural complexity and heterogeneity of native extracellular matrix without propagating free radicals.

Experimental/Methods Section:

Method. 1: Liquid cell design for photocleavage experiment

Cut out a 1 mm thick silicon gasket the size of a microscope slide (20x55 mm) with a 15x30 mm rectangular hole in the center. Sandwiched the gasket between microscope slides and clipped two small office clips near the rectangular hole, leaving about 1 cm of exposed edge on the long sides for needle to injection. Then secure the liquid cell with clipped two medium office clips to a ring stand.

Method. 2: Calculate photokinetic constants with quantitative LC-MS

Deprotected DCMAC-OH (the product of DCMAC uncaging) ranging from 0-200 μM were used for generating a standard curve by integrating LC-MS trace peak. 50 μM of DCMAC-NO-N_3 were injected into a liquid cell and incrementally dosed with light at various wavelength (365, 400, 450, and 455 nm), then analyzed by LC-MS.

Method: 3. Polymer preparation for two-photon patterning and visualization

Following previously reported with minor changes[8]. Polymer solutions were prepared in stepwise manner: PEG-BCN (3 mM) and cy5.5 (0.05 mM) were combined and stored in 37 °C for 30 min. Phosphate buffered saline (PBS), PEG-ON-DCMAC (3 mM), PEG-CHO (3 mM), aniline (10 mM), and TEG-diN3 (4.5 mM) were well-mixed with the solution and sandwiched between 2 RainX®-coated glass slides. The plates were stored in 37 °C for 30 min to form the supporting network gel and transferred to a chamber for patterning. Following patterning, the gel was stained overnight in PBS with aniline (10 mM) overnight to remove unreacted crosslinkers and replace it the next day before imaging on the Leica confocal microscope.

Figure 1.

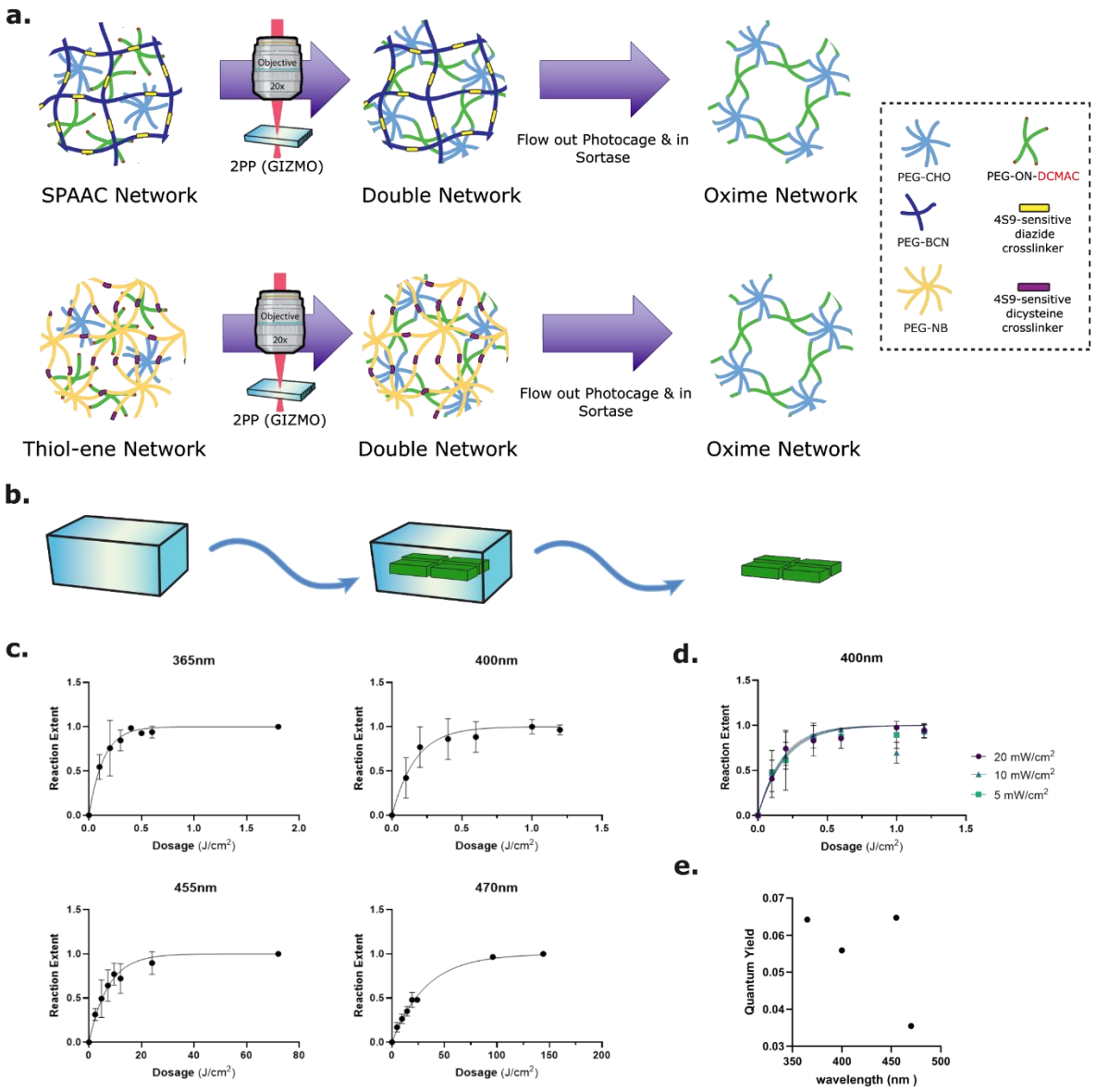

Interpenetrating networks (IPNs) formation can be controlled via two-photon lithography. a) Two distinct PEG-based networks (SPAAC or thiol-ene) construct the primary network of the IPNs. Secondary network's precursors undergo photomediated oxime ligation *via* two-photon polymerization. The patterned structure on the secondary network can be recover through sortase degradation of the primary network. b) IPNs are formed with spatial control using orthogonal networks and can be degraded to recover the patterned structure (green). c) Quantitative analysis of LC–MS peak area yields the photokinetic constant for DCMAC-NO-N_3 uncaging at 365, 400, 455, and 470 nm. d) Quantitative analysis of LC–MS peak area yields the photokinetic constant for DCMAC-NO-N_3 uncaging at 400 nm with different power intensity (5, 10, 20 mW/cm^2). Dosage can be converted into time dependent variable by multiplying to the correspond power intensity. e) single-photon quantum yield of DCMAC photouncaging at 365, 400, 455, and 470 nm.

Figure 2.

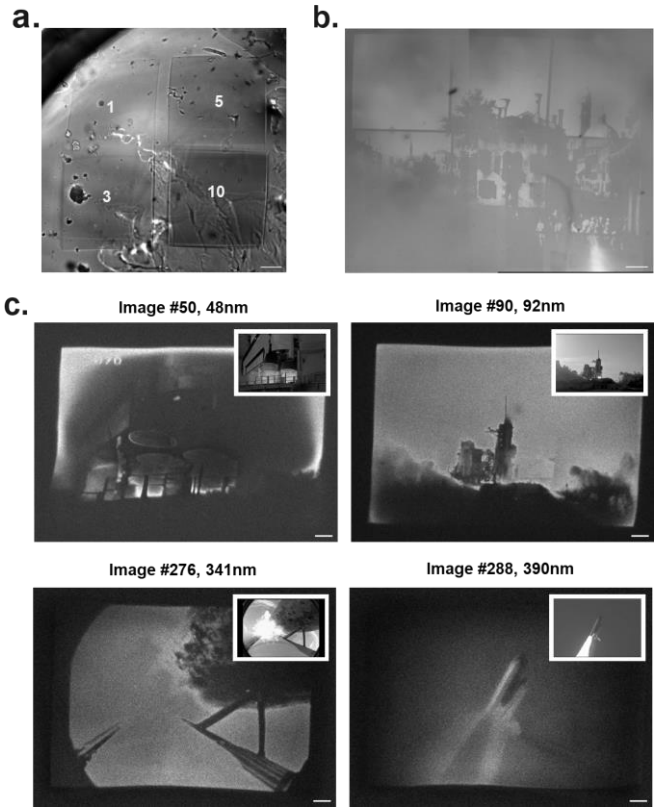

IPNs photomediated oxime ligation hydrogel via GIZMO. a) Bright field image of calibration grids with 1, 3, 5, and 10 (top to bottom repeats with a linear scanner in thiol-ene primary network). b) 2D tiled GIZMO photomediated oxime ligation in the form of "View of the Brenta, near Dolo" with thiol-ene primary network. c) Representative slices of GIZMO-patterned grayscale z-stack "flipbook" consisting of 400 planar images (450µm x 450 µm x 400 µm)), from space shuttle launching video in SPAAC primary network. Image channel scale bars are: a) Bright field,100 µm. b) 405 nm channel, 100 µm. c) 405 nm channel, 50µm.

Figure 3.

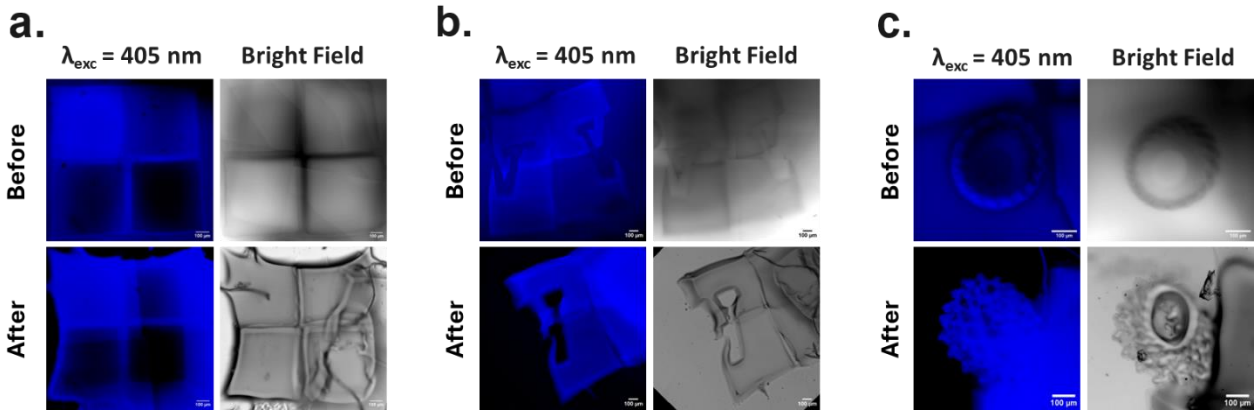

Fluorescence images at 405 nm and bright field images of patterned structure before and after release *via* sortase degradation of SPAAC primary network. a) Calibration grids. b) Vertically mirrored W. c) 3D egg structures. Scale bars are 100 µm.

References:

1. DeForest, C. A. & Anseth, K. S. Advances in Bioactive Hydrogels to Probe and Direct Cell Fate. *Annu. Rev. Chem. Biomol. Eng.* **3,** 421–444 (2012).
2. Qazi, T. H., Blatchley, M. R., Davidson, M. D., Yavitt, F. M., Cooke, M. E., Anseth, K. S. & Burdick, J. A. Programming hydrogels to probe spatiotemporal cell biology. *Cell Stem Cell* **29,** 678–691 (2022).
3. Li, W., Wang, M., Ma, H., Chapa-Villarreal, F. A., Lobo, A. O. & Zhang, Y. S. Stereolithography apparatus and digital light processing-based 3D bioprinting for tissue fabrication. *iScience* **26,** (2023).
4. Goodarzi Hosseinabadi, H., Dogan, E., Miri, A. K. & Ionov, L. Digital Light Processing Bioprinting Advances for Microtissue Models. *ACS Biomater. Sci. Eng.* **8,** 1381–1395 (2022).
5. Loterie, D., Delrot, P. & Moser, C. High-resolution tomographic volumetric additive manufacturing. *Nat. Commun.* **11,** 852 (2020).
6. Kelly, B. E., Bhattacharya, I., Heidari, H., Shusteff, M., Spadaccini, C. M. & Taylor, H. K. Volumetric additive manufacturing via tomographic reconstruction. *Science* **363,** 1075–1079 (2019).
7. Shusteff, M., Browar, A. E. M., Kelly, B. E., Henriksson, J., Weisgraber, T. H., Panas, R. M., Fang, N. X. & Spadaccini, C. M. One-step volumetric additive manufacturing of complex polymer structures. *Sci. Adv.* **3,** eaao5496 (2017).
8. Hahn, M. S., Miller, J. S. & West, J. L. Three-Dimensional Biochemical and Biomechanical Patterning of Hydrogels for Guiding Cell Behavior. *Adv. Mater.* **18,** 2679–2684 (2006).

9. Sarig-Nadir, O., Livnat, N., Zajdman, R., Shoham, S. & Seliktar, D. Laser Photoablation of Guidance Microchannels into Hydrogels Directs Cell Growth in Three Dimensions. *Biophys. J.* **96,** 4743–4752 (2009).
10. Pradhan, S., Keller, K. A., Sperduto, J. L. & Slater, J. H. Fundamentals of Laser-Based Hydrogel Degradation and Applications in Cell and Tissue Engineering. *Adv. Healthc. Mater.* **6,** 1700681 (2017).
11. Batalov, I., Filteau, J. R., Francis, R. M., Jaindl, G., Orr, L., Rapp, T. L., Yang, S., Filteau, J. A., Xie, W., Bretherton, R. C., Glaser, A. K., Liu, J. T. C., Stevens, K. R. & DeForest, C. A. Grayscale 4D Biomaterial Customization at High Resolution and Scale. 2024.01.31.578280 Preprint at https://doi.org/10.1101/2024.01.31.578280 (2024)
12. Fairbanks, B. D., Schwartz, M. P., Bowman, C. N. & Anseth, K. S. Photoinitiated polymerization of PEG-diacrylate with lithium phenyl-2,4,6-trimethylbenzoylphosphinate: polymerization rate and cytocompatibility. *Biomaterials* **30,** 6702–6707 (2009).
13. Fairbanks, B. D., Macdougall, L. J., Mavila, S., Sinha, J., Kirkpatrick, B. E., Anseth, K. S. & Bowman, C. N. Photoclick Chemistry: A Bright Idea. *Chem. Rev.* **121,** 6915–6990 (2021).
14. Eftekhari, A., de Graaf, K. R., Takmakova, E., Jongprasitkul, H., Efimov, A., Turunen, S., Kerr, A., Kellomäki, M., Luxenhofer, R., Laaksonen, T. & Durandin, N. Traceless Photopolymerization with Non-Pulsed Red Light Enables 3D-Printable Cell-Laden Hydrogels. *Adv. Mater.* **n/a,** 2502386
15. Ovsianikov, A., Mühleder, S., Torgersen, J., Li, Z., Qin, X.-H., Van Vlierberghe, S., Dubruel, P., Holnthoner, W., Redl, H., Liska, R. & Stampfl, J. Laser Photofabrication of Cell-Containing Hydrogel Constructs. *Langmuir* **30,** 3787–3794 (2014).

16. O'Hagan, M. P., Duan, Z., Huang, F., Laps, S., Dong, J., Xia, F. & Willner, I. Photocleavable Ortho-Nitrobenzyl-Protected DNA Architectures and Their Applications. *Chem. Rev.* **123,** 6839–6887 (2023).
17. Farahani, P. E., Adelmund, S. M., Shadish, J. A. & DeForest, C. A. Photomediated oxime ligation as a bioorthogonal tool for spatiotemporally-controlled hydrogel formation and modification. *J. Mater. Chem. B* **5,** 4435–4442 (2017).
18. de Gracia Lux, C., Lux, J., Collet, G., He, S., Chan, M., Olejniczak, J., Foucault-Collet, A. & Almutairi, A. Short Soluble Coumarin Crosslinkers for Light-Controlled Release of Cells and Proteins from Hydrogels. *Biomacromolecules* **16,** 3286–3296 (2015).
19. Hagen, V., Dekowski, B., Nache, V., Schmidt, R., Geißler, D., Lorenz, D., Eichhorst, J., Keller, S., Kaneko, H., Benndorf, K. & Wiesner, B. Coumarinylmethyl Esters for Ultrafast Release of High Concentrations of Cyclic Nucleotides upon One- and Two-Photon Photolysis. *Angew. Chem. Int. Ed.* **44,** 7887–7891 (2005).
20. Broguiere, N., Lüchtefeld, I., Trachsel, L., Mazunin, D., Rizzo, R., Bode, J. W., Lutolf, M. P. & Zenobi-Wong, M. Morphogenesis Guided by 3D Patterning of Growth Factors in Biological Matrices. *Adv. Mater.* **32,** 1908299 (2020).
21. Fairbanks, B. D., Schwartz, M. P., Halevi, A. E., Nuttelman, C. R., Bowman, C. N. & Anseth, K. S. A Versatile Synthetic Extracellular Matrix Mimic via Thiol-Norbornene Photopolymerization. *Adv. Mater.* **21,** 5005–5010 (2009).
22. Agard, N. J., Prescher, J. A. & Bertozzi, C. R. A Strain-Promoted [3 + 2] Azide−Alkyne Cycloaddition for Covalent Modification of Biomolecules in Living Systems. *J. Am. Chem. Soc.* **126,** 15046–15047 (2004).

23. McNitt, C. D., Cheng, H., Ullrich, S., Popik, V. V. & Bjerknes, M. Multiphoton Activation of Photo-Strain-Promoted Azide Alkyne Cycloaddition “Click” Reagents Enables in Situ Labeling with Submicrometer Resolution. *J. Am. Chem. Soc.* **139,** 14029–14032 (2017).
24. Ulrich, S., Boturyn, D., Marra, A., Renaudet, O. & Dumy, P. Oxime Ligation: A Chemoselective Click-Type Reaction for Accessing Multifunctional Biomolecular Constructs. *Chem. – Eur. J.* **20,** 34–41 (2014).
25. Grover, G. N., Lam, J., Nguyen, T. H., Segura, T. & Maynard, H. D. Biocompatible Hydrogels by Oxime Click Chemistry. *Biomacromolecules* **13,** 3013–3017 (2012).
26. Lin, F., Yu, J., Tang, W., Zheng, J., Defante, A., Guo, K., Wesdemiotis, C. & Becker, M. L. Peptide-Functionalized Oxime Hydrogels with Tunable Mechanical Properties and Gelation Behavior. *Biomacromolecules* **14,** 3749–3758 (2013).
27. DeForest, C. A. & Tirrell, D. A. A photoreversible protein-patterning approach for guiding stem cell fate in three-dimensional gels. *Nat. Mater.* **14,** 523–531 (2015).
28. Shadish, J. A., Benuska, G. M. & DeForest, C. A. Bioactive site-specifically modified proteins for 4D patterning of gel biomaterials. *Nat. Mater.* **18,** 1005–1014 (2019).
29. Wilems, T. S., Lu, X., Kurosu, Y. E., Khan, Z., Lim, H. J. & Smith Callahan, L. A. Effects of free radical initiators on polyethylene glycol dimethacrylate hydrogel properties and biocompatibility. *J. Biomed. Mater. Res. A* **105,** 3059–3068 (2017).
30. Kopyeva, I., Goldner, E. C., Hoye, J. W., Yang, S., Regier, M. C., Bradford, J. C., Vera, K. R., Bretherton, R. C., Robinson, J. L. & DeForest, C. A. Stepwise Stiffening/Softening of and Cell Recovery from Reversibly Formulated Hydrogel Interpenetrating Networks. *Adv. Mater.* **36,** 2404880 (2024).

31. Hatchard, C. G. & Parker, C. A. A new sensitive chemical actinometer - II. Potassium ferrioxalate as a standard chemical actinometer. *Proc. R. Soc. Lond. Ser. Math. Phys. Sci.* **235,** 518–536 (1956).

32. Bader, T. K., Xu, F., Hodny, M. H., Blank, D. A. & Distefano, M. D. Methoxy-Substituted Nitrodibenzofuran-Based Protecting Group with an Improved Two-Photon Action Cross-Section for Thiol Protection in Solid Phase Peptide Synthesis. *J. Org. Chem.* **85,** 1614–1625 (2020).

Supplementary Information for

3D Hydrogel Formation via a Radical-free and Multiphoton-mediated Oxime Ligation

Synthesis of N_3-PEG3-NO-DCMAC

*Synthesis of (N-11-Azido-3,6,9-trioxaundecylcarbamoyl)methoxy 2-methyl-2-propanecarbamate **1***

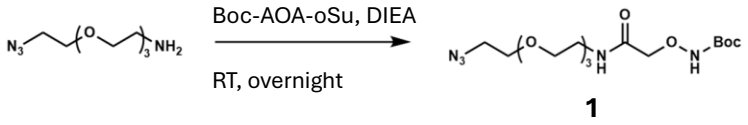

1

To a solution of N-succinimidyl [(tert-Butoxycarbonyl)aminooxy]acetate (Boc-AOA-oSu) (190 mg, 0.66 mmol, TCI America) and azido-PEG3-amine (390 mg, 1.79 mmol, BroadPharm) in 7 mL of dry DMF was added 400 µL of *N,N'*-diisopropylethylamine (DIEA) under N_2. The reaction continued overnight at room temperature, then the solvent was removed by rotary evaporation. The resulting residue was dissolved in deionized water and extracted 4x with dichloromethane. Combined organics were washed with brine and dried over anhydrous sodium sulfate. Solvent was removed by rotary evaporation and the resulting residue loaded onto a short silica column. **1** was eluted from the column using 4:1 EtOAc:hexanes (R_f = 0.19), and TLC spots did not display color after a Kaiser test (staining with 0.3% ninhydrin, 1% acetic acid in EtOH then gentle heat) indicating the absence of azido-PEG3-amine. Solvent was removed by rotary evaporation to yield 220 mg of **2** (0.56 mmol, 85%), a clear, colorless oil. ^{1}H NMR (500 MHz, $CDCl_3$): δ = 1.49 (s, 9 H), 3.38-3.42 (t, J = 4.9 Hz, 2 H), 3.50-3.55 (q, J = 5.5 Hz, 2 H), 3.59-3.63 (t, J = 5.5 Hz, 2 H), 3.64-3.71 (m, 10 H), 4.34 (s, 2 H), 5.31 (s, 1 H), 7.81 (s, 1 H). MS (ESI-MS): calculated for $C_{15}H_{30}N_5O_7$ ($[M+H]^+$): 392.215; found 392.214.

*Synthesis of N-(11-Azido-3,6,9-trioxaundecyl)(aminooxy)acetamide (N_3-PEG3-ONH_2) **2***

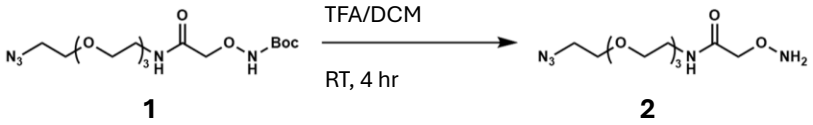

1 **2**

A solution of **1** (220 mg, 0.56 mmol) was dissolved in 3 mL of dichloromethane. 3 mL of trifluoroacetic acid were added, and the solution was stirred at room temperature for 4 hours. Solvent was removed by rotary evaporation, and the resulting residue was taken up in chloroform. The organic phase was washed with saturated sodium bicarbonate solution until no gas evolved, washed once with brine, then dried over anhydrous sodium sulfate. A TLC stain based on azide reduction by triphenylphosphine and subsequent treatment with ninhydrin showed no evidence of azide-containing compounds in the aqueous washes.[1] Solvent was removed by rotary evaporation to yield 160 mg of **2** (0.55 mmol, 98%), a clear, colorless oil. ^{1}H NMR (500 MHz, $CDCl_3$): δ = 3.39-3.44 (t, J = 5.0 Hz, 2 H), 3.51-3.56 (q, J = 5.2 Hz, 2 H), 3.59-3.62 (t, J = 5.0 Hz, 2 H), 3.63-3.70 (m, 10 H), 4.17 (s, 2 H), 4.50 (s, 1 H), 5.82 (s, 1 H), 6.84 (br. s, 2 H). MS (ESI-MS): calculated for $C_{10}H_{22}N_5O_5$ ($[M+H]^+$): 292.162; found 292.162.

*Synthesis of DCMAC-NPC **3***

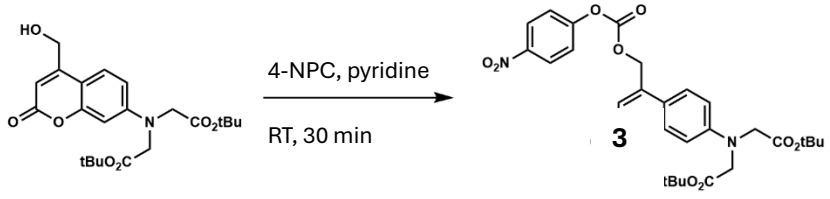

3

3 was synthesized as previously reported with slight modification.[2] Briefly, DCMAC-OH (1x) and pyridine (5x) were dissolved in dry DMF and 4-nitrophenyl chloroformate (4-NPC) (1x) in dry dichloromethane was added dropwise while stirring. After 30 minutes, solvent was removed by rotary evaporation and the resulting residue taken up in deionized water with 0.1% trifluoroacetic acid. The solution was filtered and purified by preparatory C18 HPLC using a gradient of 0-100% acetonitrile in water with 0.1% trifluoroacetic acid to yield **3**, a yellow solid, after lyophilization. MS (ESI-MS): calculated for $C_{29}H_{33}N_2O_{11}$ ($[M+H]^+$): 585.208; found 585.209.

*Synthesis of N_3-PEG3-NO-DCMAC-OtBu **4***

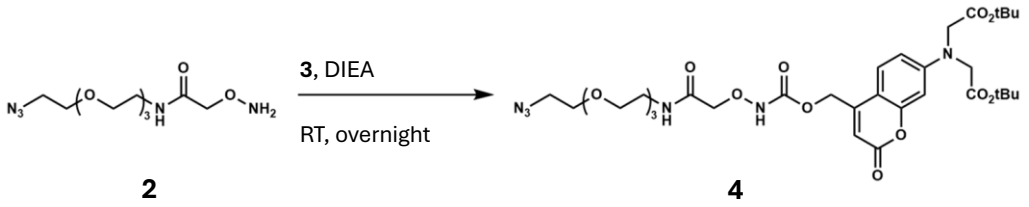

2 **4**

3 (265 mg, 0.45 mmol) was pre-activated in 5 mL of 9:1 dry DMF:pyridine and added to a solution of **2** (130 mg, 0.45 mmol) in 3 mL of 9:1 dry DMF:pyridine under N_2. The reaction was stirred at room temperature overnight. Solvent was removed by rotary evaporation, and the resulting residue was taken up in chloroform. The solution was washed with saturated sodium bicarbonate until the aqueous layer was no longer yellow, then the organic phase was washed with brine and dried over anhydrous sodium sulfate. Solvent was removed by rotary evaporation and the resulting residue purified by silica column chromatography using a gradient of 1-5% methanol in EtOAc to yield 210 mg of **4** (0.29 mmol, 63%), a yellow oil. R_f = 0.26, 5% MeOH in EtOAc. ^{1}H NMR (500 MHz, MeOD): δ = 1.48 (s, 18 H), 3.22-3.38 (m, 2 H), 3.38-3.49 (m, 2 H), 3.49-3.71 (m, 10 H), 4.18 (s, 4 H), 4.35 (s, 2 H), 4.80 (s, 2 H), 5.35 (s, 2 H), 6.13 (s, 1 H), 6.41-6.52 (m, 1 H), 6.56-6.70 (m, 1 H), 7.36-7.74 (m, 1 H), 7.98 (s, 1 H), 8.20-8.71 (d, J = 101.7 Hz, 1 H). MS (ESI-MS): calculated for $C_{33}H_{49}N_6O_{13}$ ($[M+H]^+$): 737.336; found: 737.333.

*Synthesis of N_3-PEG3-NO-DCMAC **5***

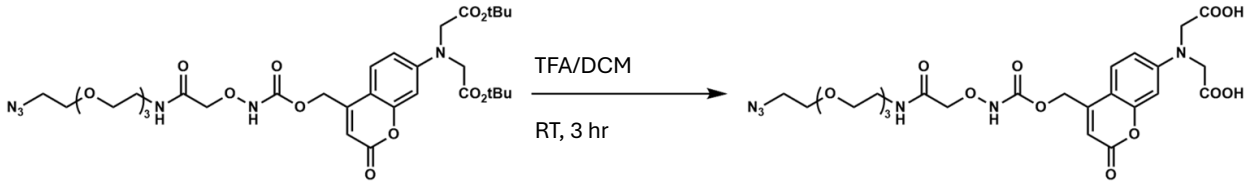

4 **5**

4 (210 mg, 0.29 mmol) was dissolved in 3 mL of dichloromethane. 3 mL of trifluoroacetic acid were added, and the solution was stirred at room temperature for 3 hours. Solvent was removed by rotary evaporation, and the resulting residue was taken up in chloroform, washed once each with saturated sodium bicarbonate and brine, then dried over anhydrous sodium sulfate. Solvent was removed by rotary evaporation to yield 180 mg of **5** (0.29 mmol, 100%), a yellow solid which was further lyophilized to help with accurate weighing. MS (ESI-MS): calculated for $C_{25}H_{33}N_6O_{13}$ ($[M+H]^+$): 625.211; found: 625.211.

Synthesis of PEG-tetra(NO-DCMAC) variants

Commercial tetraPEG precursors

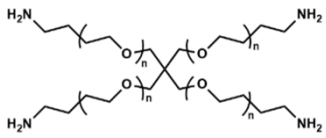

4-arm PEG-amine

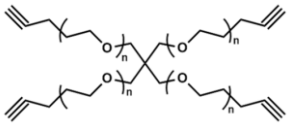

4-arm PEG-alkyne

Synthesis of PEG-tetraBCN

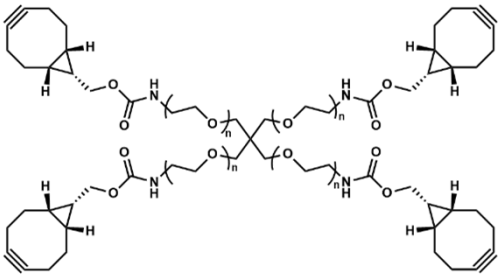

PEG-tetraBCN

PEG-tetraBCN was synthesized from 4-arm PEG-amine (10 kDa, JenKem Technology) as previously reported.[3]

*Synthesis of PEG-tetra(NO-DCMAC) **a** via CuAAC*

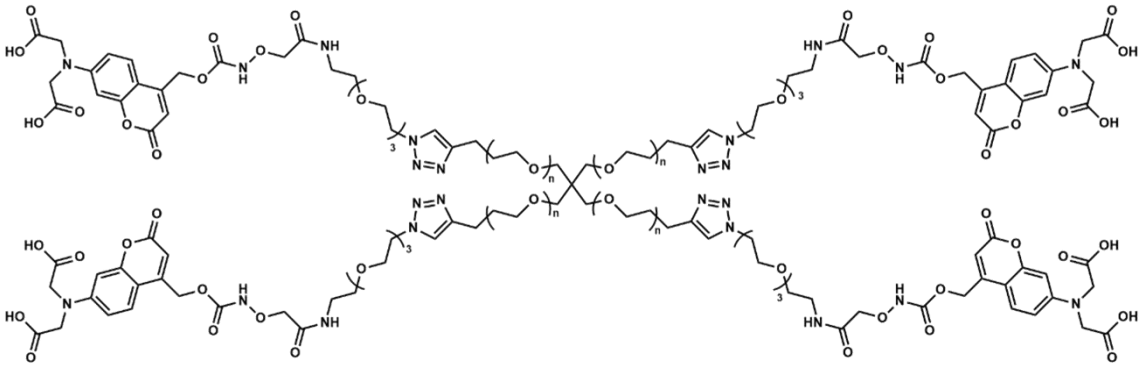

PEG-tetra(NO-DCMAC) *a*

To a 0.5 mM solution of 4-arm PEG-alkyne (1x, 10 kDa, Biopharma PEG) in phosphate-buffered saline was added sodium ascorbate (100 mM), copper sulfate dihydrate (2 mM), and **5** (4.1x). The solution was stirred overnight at room temperature, then dialyzed against a solution of 1 mM azido-PEG3-amine (BroadPharm), 10 mM sodium ascorbate, and 0.2 mM copper sulfate dihydrate in 3.5 kDa MWCO tubing overnight to block excess alkynes. The solution was further dialyzed twice against a solution of 100 mM EDTA (pH 8), twice against deionized water, and lyophilized to quantitatively yield PEG-tetra(NO-DCMAC) ***a***.

*Synthesis of PEG-tetra(NO-DCMAC) **b** via SPAAC*

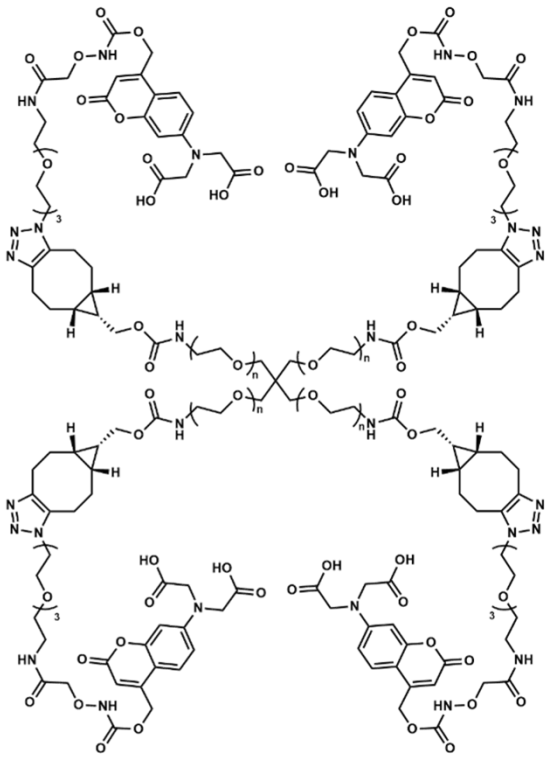

PEG-tetra(NO-DCMAC) *b*

To a 0.5 mM solution of PEG-tetraBCN (1x) in phosphate-buffered saline was added **5** (4.1x). The solution was mixed and incubated at 37 °C for 1 hour, then dialyzed against 1 mM azido-PEG3-amine (BroadPharm) in 3.5 kDa MWCO tubing overnight to block excess alkynes. The solution was further dialyzed twice against deionized water and lyophilized to quantitatively yield PEG-tetra(NO-DCMAC) ***b***.

Functionalization extent of 4-arm PEG-NO-DCMAC *a* and *b*

Quick method – Absorbance at 365 nm

Lyophilized ***a*** and ***b*** were dissolved at known concentrations in deionized water and absorbance measurements taken on a Nanodrop 2000 using a quartz cuvette with 1 cm path length. Absorbance at 365 nm was collected and a Beer-Lambert calculation was performed using the known extinction coefficient for DCMAC (ε_{365} = 16000) to estimate the total concentration of photocage groups present in the solution. This was divided by 4[PEG-NO-DCMAC] (expected concentration accounting for tetravalent PEG) to estimate the extent of functionalization.

Accurate method – NMR

The baseline-corrected integration of ^{1}H NMR peaks (500 MHz, $CDCl_3$) corresponding to DCMAC (2 H) were compared to peaks corresponding to the pentaerythritol core in ***a*** and ***b*** (8 H). This ratio was used to calculate functionalization extent of the PEGs.

Synthesis of PEG-CHO:

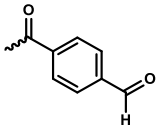

was synthesized as previously reported with minor changes[4]. 4-formylbenzoic acid (2.2 mmol) was combined with HATU (2 mmol), DIEA (5 mmol), and DMF under nitrogen for 10 min in a round-bottle flask. In parallel, 8-arm PEG-amine (1 mmol) was dissolved in DMF containing DIEA (5 mmol). The two solutions were mixed and purged with nitrogen for 10 min. The reaction was stirred overnight at room temperature. Reaction was precipitated with ethyl ether. dH_2O was added to the reaction and the solution was transferred to dialysis tubing and dialyzed for 24 hours in dH_2O. The solution was filtered through a syringe filter and lyophilized to obtain a white powder.

References

1. Cegielska, B. & Kacprzak, K. Simple and Convenient Protocol for Staining of Organic Azides on TLC Plates by Ninhydrin. A New Application of an Old Reagent. *Chem. Anal.* **54**, 807–812 (2009).
2. Broguiere, N. *et al.* Morphogenesis Guided by 3D Patterning of Growth Factors in Biological Matrices. *Advanced Materials* **32**, 1908299–1908299 (2020).
3. DeForest, C. A. & Tirrell, D. A. A photoreversible protein-patterning approach for guiding stem cell fate in three-dimensional gels. *Nature Materials* **14**, 523–531 (2015).
4. Richardson, B. M. *et al.* Viscoelasticity of hydrazone crosslinked poly(ethylene glycol) hydrogels directs chondrocyte morphology during mechanical deformation. *Biomater. Sci.* **8**, 3804–3811 (2020).